Eur. Phys. J. B **59**, 463–469 (2007)
DOI: 10.1140/epjb/e2007-00083-9

THE EUROPEAN PHYSICAL JOURNAL B

Hard axis magnetic field dependence on current-induced magnetization switching in MgO-based magnetic tunnel junctions

Y. Saito[1,a], T. Inokuchi[1], H. Sugiyama[1], and K. Inomata[2]

[1] Corporate R & D Center, Toshiba Corporation, 212-8582 Kawasaki, Japan
and
CREST, Japan Science and Technology Agency (JST), Kawaguchi, 332-0012 Saitama, Japan
[2] National Institute for Materials Science, 1-2-1, Sengen, 305-0047 Tsukuba, Japan
and
CREST, Japan Science and Technology Agency (JST), Kawaguchi, 332-0012 Saitama, Japan

Received 28 September 2006 / Received in final form 15 February 2007
Published online 28 March 2007 – © EDP Sciences, Società Italiana di Fisica, Springer-Verlag 2007

Abstract. We conducted a detailed study of hard axis magnetic field (H_{hard}) dependence on current-induced magnetization switching (CIMS) in MgO-based magnetic tunnel junctions (MTJs) with various junction sizes and various uniaxial anisotropy fields. The decreases in critical current density (J_c) and the intrinsic critical current density (J_{c0}) estimated from the pulse duration dependence on J_c in CIMS are observed when applying H_{hard} for all MTJs. The decrease in energy barrier of CIMS is also observed except for the largest sample. These results indicate that the reduction of J_c is attributable to both the increase of spin-transfer efficiency and the decrease in energy barrier in the case of applying H_{hard}. The J_{c0} decreases with increase in the mutual angle between the direction of magnetization and the easy axis (θ_f), which is consistent with the theoretical prediction proposed by Slonczewski. The degree of the reduction of J_{c0} for the same value of H_{hard} decreases with decreasing size of MTJs. This behavior is considered to be related to not only decrease in θ_f due to the increase in anisotropy field in MTJs, but also to the increase in the variance of the initial angle of magnetization due to the thermally activated magnon excitation. The stable switching endurance related to CIMS was observed in a wide range of MTJ sizes when applying H_{hard}. Moreover, we proposed a new architecture and a new switching method considering write disturbance. These results would be useful for application to spin memory and other spin-electronic devices.

PACS. 72.25.-b Spin polarized transport – 72.25.Hg Electrical injection of spin polarized carriers – 73.43.Qt Magnetoresistance – 73.63.-b Electronic transport in nanoscale materials and structures – 75.47.-m Magnetotransport phenomena; materials for magnetotransport

1 Introduction

Current-induced magnetization switching (CIMS) has been extensively studied in recent years, since the possibility of reversing the magnetization of a free layer in a multilayered structure with a current perpendicular to the plane was predicted by Slonczewski and Berger [1,2]. CIMS has a potential technological application to spin-electronic devices. However, critical current density (J_c) needed for deterministic switching for magnetization of a free (storage) layer is very large ($>10^7$ A/cm^2) for typical magnetic tunnel junctions (MTJs) and low J_c is required in order to achieve low power consumption, high density and high reliability in tunnel barrier for the application of CIMS to spin-electronic devices. To date, several studies [3–7] have been conducted with a view to reducing J_c in MgO-based MTJs. The basic equation that describes superparamagnetism is the Arrhenius-Neel equation, which describes the probability per unit time of hopping from one magnetic potential well to another over an energy barrier. Simple analysis of this equation shows that $K_uV/k_BT > 50$ is the stability criterion for an acceptably long data lifetime, considered to be as long as 10 years at room temperature, where K_u is uniaxial anisotropy constant, V is volume of free layer, k_B is the Boltzmann constant, and T is the temperature. However, spin-electronic devices such as spin RAM have many MTJ cells $>256 \times 10^6$ bits and it is essential to guarantee non-volatility at temperature >353–393 K, which depends on the applications. Therefore, K_uV/k_BT should be larger than 60–80, and further reduction of J_c is required, taking into account the thermal stability parameters $K_uV/k_BT > 60-80$ necessary to guarantee non-volatility.

[a] e-mail: yoshiaki.saito@toshiba.co.jp

Recently, we [8] and another group [9] showed the reduction of J_c when applying hard axis (transverse) magnetic field (H_{hard}) in MTJs and GMR nano pillar, respectively. Moreover, increase in the switching speed was confirmed [9] when increasing the initial angle of the magnetization accompanying increase of H_{hard}, which was predicted by Sun [10]. Scientifically, the effect of H_{hard} on CIMS is also interesting, because the increase of the efficiency (η) of spin injection with a mutual angle between the direction of magnetization and the easy axis, and decrease in J_c ($\propto 1/\eta$) were predicted theoretically [1,11]. The decrease in energy barrier of CIMS due to the magneto-static energy is also expected when applying H_{hard} in MTJs.

The present study reports further details of H_{hard} dependence of J_c. In particular, we present the H_{hard} dependence of CIMS in MgO-based MTJs with various junction sizes and uniaxial anisotropy field of the free layer (H_k).

2 Experimental procedure

The MgO-based MTJs with bottom pinned structure were prepared on thermally oxidized Si wafers by using UHV magnetron sputtering system with a base of pressure less than 2×10^{-9} Torr. The structure used here is bottom electrode (400 nm)/Ta (10 nm)/Ru (5 nm)/IrMn (10 nm)/CoFe (3 nm)/Ru (0.9 nm)/CoFeB (4 nm)/MgO (1.05–1.1 nm)/CoFeB (2 nm)/Ta (5 nm)/Ru (10 nm)/top electrode (430 nm). After post-annealing of the films, crystallization of CoFeB layers was confirmed by transmission electron microscopy images. The junctions were patterned into deep sub-micron sizes by using a photolithography step and resist slimming to define the current perpendicular (CPP) MTJ structure. The resist slimming was performed by using inductively coupled oxygen plasma. After and before resist slimming, uniform slimming of resist between width (W) and length (L) in MTJs was confirmed by scanning electron microscopy (SEM) images. A slimmed resist pattern was transferred to the Ta mask by SF_6 reactive ion etch (RIE) steps and stopped at the top Ru layer and then the MTJ film was etched by Ar ion milling. After etching, the SiO_X protection layer was deposited. The photo-resist is then stripped, and a second RIE step is carried out for defining the bottom electrode. After this step, a SiO_2 film of about 300 nm is blanket coated with O_2 reactive sputtering. Following this step, the sample is coated with 400 nm of OFR-5EB photoresist and hard baked. The resist coating provides the necessary planarization of the surface. The SiO_2 on top of MTJs is then selectively etched back by CHF_3 plasma, stopping on the top Ta mask, thus opening up the junction for top wiring. The samples are then sputter coated with Ti/AlCu/Ti for top-level contact, and top electrode of Ti/AlCu/Ti was patterned into wiring using photolithography. The shape of MTJ was designed to be rectangular, but the actual shape was wavey due to the optical proximity effect. The actual element area was estimated from the RA (resistance-area product) value. Uniformity of the absolute value of RA value and MR ratio was confirmed in a chip by measuring many MTJs with more than 1000 nm width and various aspect ratios (L/W) covering $L/W = 1{-}5$. As described before, we also confirm the absolute values of the resist slimming between W and L are the same by SEM images. From these results, we can estimate the actual sizes of MTJs precisely, taking into account the optical proximity effect observed in SEM images. The junction area of MTJs ranged from 0.164 to 0.00426 μm^2 and the actual junction width W was from 65 to 350 nm and aspect ratio was $L/W \sim 1 \sim 2.5$. MTJs with three different RA values were prepared. Typical value of magneto-resistance (MR) and RA for $H_{hard} =$ 0 Oe in MTJs is MR = 65%, RA = 6 $\Omega\,\mu m^2$ for Sample#1, MR = 105%, RA = 17 $\Omega\,\mu m^2$ for Sample#2 and MR = 80.3%, RA = 13.5 $\Omega\,\mu m^2$ for Sample#3, respectively. These MTJs have various coercivities (H_C) from 30 to 90 Oe and anisotropy field (H_K) from 30 to 150 Oe. The H_K values were estimated from the fitting of measured astroid curves to Stoner-Wohlfath astroid equation.

CIMS was measured at room temperature using the DC four-point probe method after applying short current pulses with durations from 10 μs to 10 ms, and detailed H_{hard} dependence on CIMS in MTJs with various widths was investigated. The interval between the write short current pulses was set at over 100 ms in order to eliminate the effects of Joule heating of the samples. In a series of experiments of H_{hard} dependences on J_c, a magnetic field of H_{easy} was fixed at the center of an M-H curve, because independence of average value of Jc has been reported for the value of H_{easy} [1,12,13].

3 Results and discussions

Figures 1a and 1b show the results of (a) resistance as a function of amplitude of pulse current ($R{-}I$ curve) under a magnetic field applied along easy axis of a free layer $H_{easy} = -72$ Oe and $H_{hard} = 0$ Oe and (b) corresponding resistance as a function of H_{easy} ($R{-}H_{easy}$ curve) under $H_{hard} = 0$ Oe for Sample#1 with RA value of 6 $\Omega\,\mu m^2$ in the case of $H_{hard} = 0$ Oe. The sweep direction of the pulse current for $R{-}I$ curve is shown in Figure 1a. A sharp jump from high resistance state to low resistance state was observed at critical current $I_C^- = -1.78$ mA and a sharp jump from low resistance state to high resistance state was observed at $I_C^+ = 2.83$ mA. The change of resistance (ΔR) observed in $R{-}I$ curve corresponds to the value of ΔR in $R{-}H_{easy}$ curve. This correspondence of ΔR means that the magnetization is sufficiently switched through spin-polarized current.

Figures 2a and 2b show the typical $R{-}I$ curve and typical $R{-}H_{easy}$ curve for applying H_{hard}, respectively, in MTJ of Sample#1. Figures 2a and 2b are the case of $H_{hard} = -15$ Oe, and the value of H_{easy} was -13 Oe for measuring $R{-}I$ curve. The MR ratio decreased to 20.5% corresponding to the rotation of magnetization [12]. As shown in Figure 2b, when decreasing H_{easy} from -50 Oe to 0 Oe in $R{-}H_{easy}$ curve, the resistance gradually decreases due to the rotation of magnetization, and for

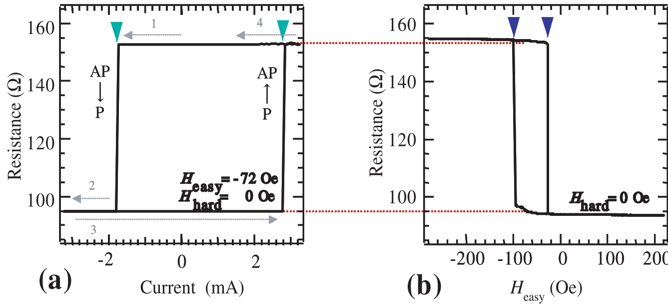

Fig. 1. (a) Typical resistance versus amplitude of pulse current (R–I curve) under a magnetic field $H_{easy} = -72$ Oe in the case of $H_{hard} = 0$ Oe, and (b) typical resistance versus H_{easy} (R–H_{easy} curve) in the case of $H_{hard} = 0$ Oe for Sample#1 with RA value of 6 $\Omega\,\mu\text{m}^2$ and 170 nm MTJ width.

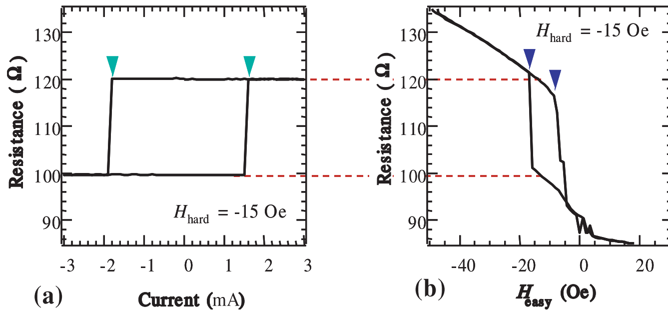

Fig. 2. Typical R–I curve and typical R–H_{easy} curve in the case of applying $H_{hard} = 15$ Oe, and $H_{easy} = -13$ Oe for Sample#1 with RA value of 6 $\Omega\,\mu\text{m}^2$ and 170 nm MTJ width.

$H_{easy} \sim 0$ Oe, the magnetization of free layer has initial angle (θ_f) from the easy axis of a pinned layer of MTJ. In the case of applying H_{hard}, ΔR observed in R–I curve also corresponds to the value of ΔR in R–H_{easy} curve. This correspondence of ΔR means that the magnetization is also sufficiently switched through spin-polarized current between θ_f and $\pi - \theta_f$ in the case of applying H_{hard}.

Figure 3a shows the H_{hard} dependence on R–I curves for several values of H_{hard} in MTJ of Sample#1. The pulse duration used in this measurement was 1.0 ms. The decrease in the value of J_c with increasing H_{hard} is observed.

In order to investigate the origin of the reduction of J_c when applying H_{hard}, the dependence of J_c on pulse duration for several values of H_{hard} was measured. Figures 3b and 3c show the examples of J_c dependence on pulse duration for Sample#1. As shown in Figures 3b and 3c, the absolute value of J_c decreases with increasing the intensity of H_{hard}. The increase of absolute value of J_c is also observed as the pulse duration decreases. The intrinsic critical current density ($J_{c0}^{\pm}$), derived from the model of thermally activated CIMS, is expressed [14] as

$$J_c^{\pm} = J_{c0}^{\pm}\left[1 - (k_BT/E^{\pm})\ln(t_p/t_0)\right] \quad \text{for} \quad t_p \gg t_0, \quad (1)$$

where t_0 is the inverse of the attempt frequency, t_p is the pulse duration, and $E^{\pm}$ is the actual barrier height that the spin experiences during the magnetization reversal process. The intrinsic critical current density $J_{c0} = (I_{c0}^{+} - I_{c0}^{-})/2A$, and $E^{ave}/2k_BT = (E^{+} + E^{-})/2k_BT$, ob-

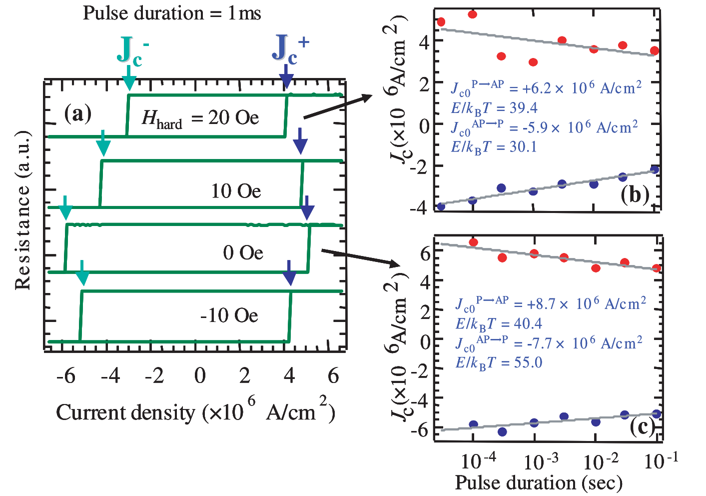

Fig. 3. (a) H_{hard} dependence on R–I curves for several values of H_{hard}; (b) and (c) show the example of J_c dependence on pulse duration in the case of $H_{hard} = 20$ Oe and $H_{hard} = 0$ Oe, respectively, for Sample#1 with RA = 6 $\Omega\,\mu\text{m}^2$ and 150 nm MTJ width.

tained by the fitting shown in Figures 3b and 3c to equation (1) of thermally activated CIMS are shown in Table 1. Note that the estimated J_{c0} significantly decreases from 8.2×10^6 A/cm^2 ($H_{hard} = 0$ Oe) to 6.0×10^6 A/cm^2 ($H_{hard} = 20$ Oe). The value of $E^{ave}/2k_BT$ also decreases with increase of H_{hard} from 47.7 ($H_{hard} = 0$ Oe) to 34.7 ($H_{hard} = 20$ Oe). A difference in the activation energies between E^+ and E^- for current switching for the two cases of P to AP and of AP to P was observed as shown in Figure 3. At $H_{hard} = 0$ Oe, the activation energy of AP to P is larger than that of P to AP. On the other hand, in the case of thermal activation energy for large-size samples (620×620 nm^2 and 320×1120 nm^2) which was measured using magnetic field sweep rate by means of external and current induced magnetic fields through the word line, the activation energy of P to AP is always larger than that of AP to P (Please refer to Fig. 2 in [15] and Fig. 2 in [16]). The difference of activation energy between AP to P and P to AP might be correlated to the ratio of strength of stray field/orange peel coupling, which would stabilize AP to P and P to AP, respectively. However, we think that more efforts in experimental and theoretical works are necessary in order to fully understand the difference between E^+ and E^-.

In order to confirm the origin of the decrease in J_c, we measured the I_c dependence on pulse duration for the several MTJs with different size and RA values. Figure 4 shows the I_c dependence on pulse duration for MTJ (Sample#2) with RA = 17 $\Omega\,\mu\text{m}^2$ and 180 nm MTJ width. In Sample#2 and Sample#3, we cannot measure CIMS at $H_{hard} = 0$ Oe due to the breakdown of tunnel barrier in MTJs. The value of J_c at $H_{hard} = 0$ Oe is over 1.1×10^7 A/cm^2 in Sample#2 and Sample#3. The absolute value of I_c decreases with increasing the intensity of H_{hard}. The increase of absolute value of I_c is also observed as the pulse duration decreases. The intrinsic critical current density J_{c0} and $E^{ave}/2k_BT$, obtained by the

Table 1. The estimated J_{c0} and energy barrier of CIMS from the pulse duration dependence on J_c in Sample#1∼Sample#3 under H_{hard}.

	H_{hard} (Oe)	J_{c0}^{ave} (A/cm^2)	E^{ave}/k_BT
Sample#1	0	8.2×10^6	47.7
(RA = 6 $\Omega\,\mu$m^2)	20	6.0×10^6	34.7
Sample#2	–17	7.4×10^6	41.0
(RA = 17 $\Omega\,\mu$m^2)	–21	6.7×10^6	35.0
	–26	3.9×10^6	29.0
Sample#3	–10	1.2×10^6	29.0
(RA = 13.5 $\Omega\,\mu$m^2)	–15	1.1×10^6	34.3
	–20	8.6×10^5	29.9

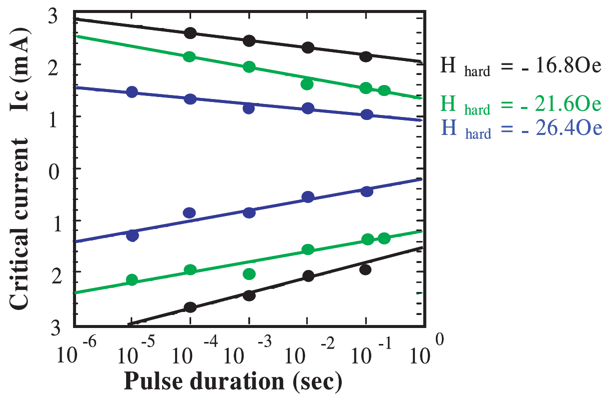

Fig. 4. Critical current (I_c) dependence on pulse duration in the case of $H_{hard} = -16.8$ Oe, -21.6 and -26.4 Oe for Sample#2 with RA = 17 $\Omega\,\mu$m^2 and 180 nm MTJ width.

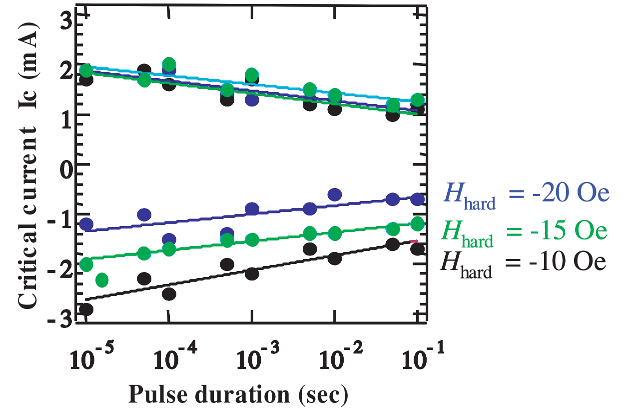

Fig. 5. Critical current (I_c) dependence on pulse duration in the case of $H_{hard} = -10$ Oe, -15 and -20 Oe for Sample#3 with RA = 13.5 $\Omega\,\mu$m^2 and 350 nm MTJ width.

fitting shown in Figure 4 to equation (1) of thermally activated CIMS are also shown in Table 1. In the case of Sample#2, the decrease in J_c also originates from both J_{c0} and $E^{ave}/2k_BT$.

We show another example of I_c dependence on pulse duration for MTJ (Sample#3) with RA = 13.5 $\Omega\,\mu$m^2 and 350 nm MTJ width in Figure 5. This sample has the largest size for which we can measure CIMS such that the absolute value of ΔR observed in R–I curve is nearly the same as that of ΔR in R–H_{easy} curve. The absolute value of I_c decreases with increasing the intensity of H_{hard}. The increase of absolute value of I_c is also observed as the pulse duration decreases. The J_{c0} and $E^{ave}/2k_BT$, obtained by the fitting shown in Figure 5 to the equation (1) are also shown in Table 1. In the case of large-size sample, J_{c0} decreases with increase of H_{hard}. However, in terms of activation energy, $E^{ave}/2k_BT$ does not decrease monotonously with increase of H_{hard}.

Thus, the observed $E^{\pm}/k_BT$ decreases monotonously as $|H_{hard}|$ increases except for the largest sample. Assuming a single-domain model, the magneto-static energy of a free layer E_s is expressed as $E_s(\theta_f) = K_u \sin^2\theta_f - M_sH_{easy}\cos\theta_f - M_sH_{hard}\sin\theta_f$, where θ_f is the mutual angle between the direction of magnetization and the easy axis. Therefore, the average barrier height E^{ave} should decrease as $|H_{hard}|$ increases. The discrepancy between the experimental result and the theory derived from a single-domain model in the case of the largest sample is considered to be the effect of the multidomain formation, because applying H_{hard} affects the structure of domain [17]. As is well-known, a 2 mA vertical and uniform current through the junction will produce a circular vortex field (Oersted field) of 5 Oe at the periphery of MTJ having the size of 1.0 μm^2. The Oersted field would affect the structure of domain even in MTJ with the size of 0.164 μm^2.

On the other hand, from the results of pulse duration dependence on critical current density, the decreases in J_c and J_{c0} are observed, when applying H_{hard} in all samples.

The J_{c0} in the presence of H_{easy} is expressed as follows [10]:

$$J_{c0} = \frac{\alpha}{\eta}\left(\frac{2e}{\hbar}\right)(l_mH_kM_s)\left(1 + \frac{H_{easy}}{H_k}\right), \tag{2}$$

where α is the damping constant, η is the spin-transfer efficiency, e is the electron charge, $\hbar$ is the reduced Planck constant and l_m is the thickness of the free layer. η [1] is given as

$$\eta = (p/2)/(1 + p^2\cos\theta), \tag{3}$$

where p is the tunneling spin polarization of pinned layer and θ is the angle between the moments of the pinned

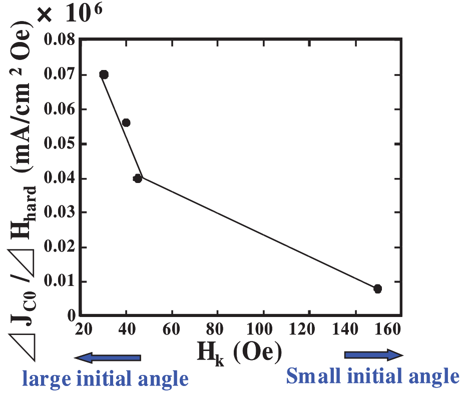

Fig. 6. Degree of decrease in J_{c0} as a function of H_k of free layer for 4 MTJs (Sample#1 and #2) with various H_k.

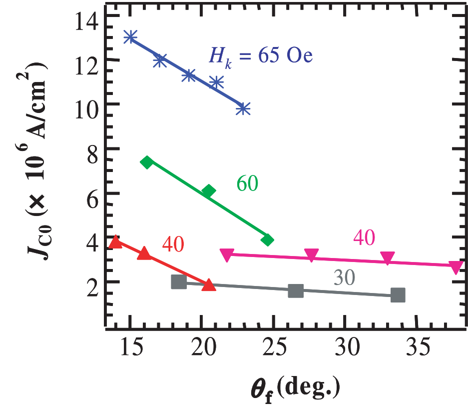

Fig. 7. Estimated J_{c0} as a function of mutual angle between the direction of magnetization and the easy axis (θ_f) for MTJs with various H_k for 5 MTJs (Sample#1 and #2) with various H_k.

layer and the free layer. By analogy with equation (2), the reduction of J_{c0} in the case that H_{hard} is applied can be explained by the increase of η because applying H_{hard} causes θ to be out of alignment from 0 or π, though the dependence of J_{c0} on H_{hard} is not accounted for in equation (2).

The degree of the reduction of J_{c0} for the same value of H_{hard} decreases with decrease of size in MTJs. Figure 6 shows the degree of decrease in J_{c0} as a function of H_k of free layer. The degree of the dependence of decrease of J_{c0} on H_{hard} decreases with increase of H_k. The mutual angle between the direction of magnetization and the easy axis (θ_f) can be estimated using

$$\theta_f = \tan^{-1}\left(H_{hard}/H_k\right). \quad (4)$$

Therefore, Figure 6 indicates that the degree of the dependence of decrease of J_{c0} on H_{hard} depends on θ_f. These results indicate the increase in spin-transfer efficiency (η) for increasing θ_f. This result is consistent with the theory [1,11]. From the equation (3), J_{c0} should decrease with increase of θ_f. For MTJs with large H_k value, $\theta_f = \tan^{-1}(H_{hard}/H_k)$ is smaller than that for MTJs with small H_k value. Therefore, degree of decrease of J_{c0} for MTJ with large H_k value should be smaller than that for MTJ with small H_k value. Figure 7 shows the estimated J_{c0} from the pulse duration dependence on J_c as a function of θ_f for MTJs with various H_k. For all samples, J_{c0} decreases with increase in θ_f. Figure 7 indicates that the degree of decrease in J_{c0} in the region of $\theta_f < 20$ degree is larger than that in the region of $\theta_f > 20$ degree. This result suggests that small θ_f is enough for the decrease in J_{c0}. However, from the equation (3), J_{c0} has dependence of $\cos\theta_f$. This equation means that the degree of J_{c0} in the region of large θ_f should be larger than that of small θ_f. Recently, Slonczewski has proposed [11] that η is proportional to $\sin\theta_f$ in the case of MTJs in the condition of constant voltage. However, this relationship is also not enough to explain the results in Figure 7. This inconsistency might be related to the effect of the micromagnetic domain formation and/or the effect of thermally activated magnon excitation as shown below.

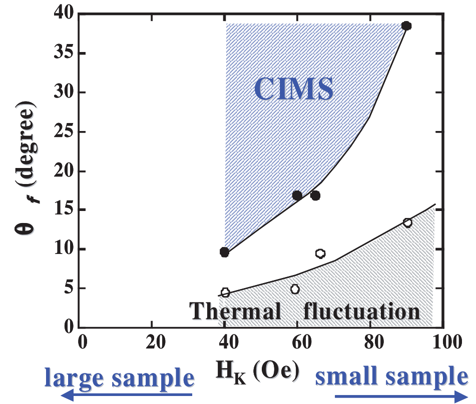

Fig. 8. H_k dependences on θ_f estimated using $\theta_f = \tan^{-1}(H_{hard}/H_k)$ in MTJs (Sample#2) with RA = 17 $\Omega\,\mu$m^2. In the blue region, CIMS is observed for the measuring condition of the limitation of the maximum current flow of $J = 1 \times 10^7$ A/cm^2. The values of estimated θ_{FT} are also plotted in the thermal fluctuation region.

Figure 8 shows H_k dependence on θ_f estimated using $\theta_f = \tan^{-1}(H_{hard}/H_k)$. In this blue region, CIMS is observed in the condition of limitation of the maximum current flow of $J = 1 \times 10^7$ A/cm^2. This figure indicates that larger H_{hard} is required for decrease in J_c for small sample than in the case of the large sample. There are two reasons for this property. One is the requirement of large H_{hard} for obtaining the same value of θ_f as for small sample, because small sample has large H_k. Another reason is considered to be the thermal fluctuation of magnetization because spin moment would be thermally fluctuated with the angle of θ_{FT} [18]. θ_{FT} can be estimated by using

$$\theta_{FT} = \left(\frac{k_B T}{\mu_0 H_k M_S V}\right)^{1/2}, \quad (5)$$

where V is the volume of free layer in MTJs. The values of estimated θ_{FT} are plotted in Figure 8. In this thermal fluctuation region, applying H_{hard} is meaningless in terms of reducing J_c. Figure 8 also suggests that necessary

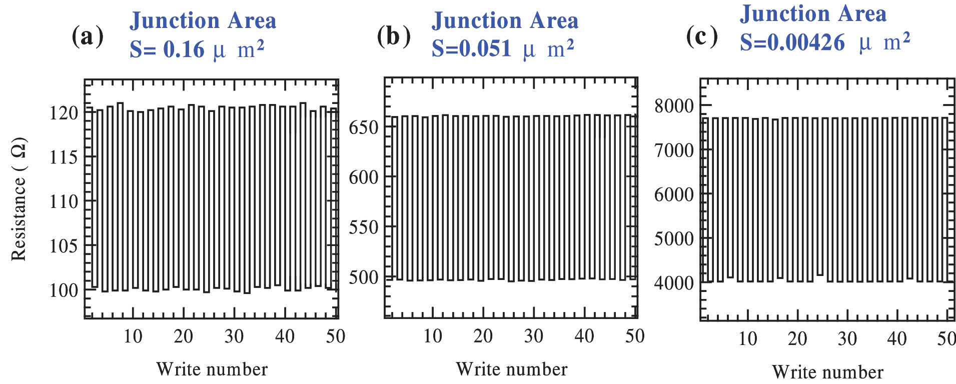

Fig. 9. Size dependence on the result of switching reproducibility under H_{hard} for (a). Junction area $S = 0.16$ μm^2 (W = 350 nm^2, $H_k = 30$ Oe), (b) $S = 0.051$ μm^2 (W = 180 nm^2, $H_k = 60$ Oe) and (c) $S = 0.00426$ μm^2 (W = 65 nm^2, $H_k = 90$ Oe).

θ_f for reduction of J_c is about twice θ_{FT}. Thus the behavior in Figure 8 is considered to be related to not only decrease in the mutual angle (θ_f) of magnetization due to the increase in anisotropy field H_k, but also to the increase in the variance of the initial angle of magnetization θ_{FT} due to the thermally activated magnon excitation. In Figure 7, we cannot observe the decrease in J_{c0} in the region of $0 < \theta_f < 13$ degree. This would also be due to the thermally activated magnon excitation. More experimental work such as measurement in a low-temperature region is necessary in order to fully understand the data in Figure 7.

Next, we would like to describe the results of switching reproducibility. Figures 9a–9c show the size dependence on the result of switching reproducibility. The stable switching endurance related to CIMS was observed when applying H_{hard} to a wide range of MTJ sizes. In this measurement, the pulse duration was 100 μs, and H_{hard} is -15 Oe, -22 Oe and -38 Oe for junction area $S = 0.16$ μm^2 (W = 350 nm^2, $H_k = 30$ Oe), $S = 0.051$ μm^2 (W = 180 nm^2, $H_k = 60$ Oe), $S = 0.00426$ μm^2 (W = 65 nm^2, $H_k = 90$ Oe), respectively. As is well-known, a 2 mA vertical and uniform current through the junction will produce an Oersted field of 5 Oe at the periphery of MTJ having the size of 1.0 μm^2. When increasing the value of vertical current, the strength of Oersted is sufficient to induce a vortex state, which leading to observing half the absolute value of resistance change (ΔR) induced by CIMS compared with ΔR induced by external magnetic field [19]. In the same samples of Sample#3, when increasing current, we also observed the vortex state at $H_{hard} = 0$ Oe, whereas, in most samples, the breakdown voltage of tunnel barrier is much smaller than the voltage observed in a vortex state. In the case of the largest sample and $H_{hard} = 0$ Oe, we cannot observe a stable switching reproducibility. The value of resistance change has a variation and the probability of switching by CIMS is very low. This would be because a stronger positive vortex field never induced a transition back to the low-resistance parallel state as noted in reference [19]. When applying H_{hard}, we can observe stable switching reproducibility as shown in Figure 9. These results indicate that the absolute value of the current that CIMS induces becomes smaller than the current value that the vortex state induces by applying a magnetic field to a hard axis. Therefore, a hard axis field helps suppress the probability of inducing the vortex state even in a relatively large sample. In all results, we confirmed that the correspondence of ΔR between R–I curves and ΔR in R–H_{easy} curves, which means that the magnetization is sufficiently switched through spin-polarized current. All these results suggest that a CIMS method is applicable for MTJ with $W \leq 350$ nm, whereas, the vortex state is generally not a problem in the smaller devices that will have to be employed in future high-density spin-electronic devices such as spin-transfer switched MRAM cells.

Finally, we would like to explain how we propose to employ a pulsed hard axis magnetic field to reduce J_{c0} for the spin-transfer switched MRAM cells in a manner that would not result in an unacceptable level of thermal activation energy ($E^{ave}/2k_BT$). As shown above, the decreases in J_c, J_{c0} and also in thermal activation energy are observed when applying H_{hard}. In general, MRAM cells use the half selection method for write operation in which an additional metal line (digit line) is necessary, which increases the MRAM cell size and induces the write disturbance due to the reduction of $E^{ave}/2k_BT$, when employing a pulsed hard axis field. Therefore, the additional digit line is not favorable in the case of employing a pulsed hard axis magnetic field to reduce J_{c0}. The architecture shown in Figure 10a [20] is one of the possibilities with no digit line for employing a pulsed hard axis magnetic field to reduce J_{c0}, whereas the easy axis direction is different between Figure 10a and the architecture in reference [20]. A magnetic field, which has been generated by the bottom electrode and bit line, has been utilized for reduction of J_{c0}. However, this architecture also has a possibility of reducing thermal activation energy due to the write disturbance of magnetic field generated by bit line. We propose a new architecture shown in Figure 10b, which has another thicker bit line above the top electrode, which has no write disturbance. When we assume the distance of 45 nm between top of MTJ and bottom of top electrode, MTJ size of 120 × 240 nm^2, MTJ write current density of 1.0×10^6 A/cm^2 and use of yoke wiring for top and bottom electrodes, a hard axis magnetic field is

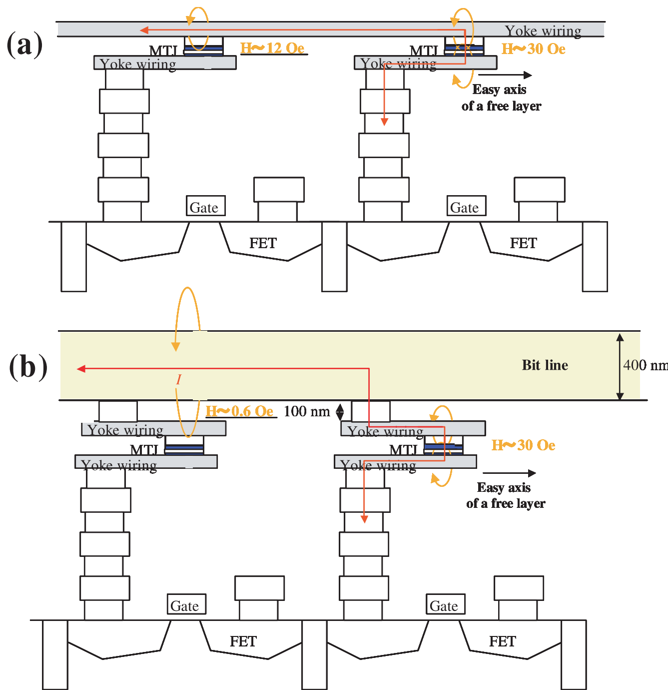

Fig. 10. (a) Device structure for applying H_{hard} to MTJ by using write current [20]; (b) improved device structure for applying H_{hard} to MTJ by using write current. The architecture (b) can avoid half-selection problem.

estimated to be 31 Oe. For example, MTJ with H_k = 75 Oe, $\theta_f = 22.5$ degree can be estimated by using equation (4). This initial angle would be enough for reduction of J_{c0}. Another approach with a possibility of reducing J_{c0} for the spin-transfer switched MRAM cells is the use of exchange biased free layer, which would have large value of thermal activation energy. When changing the thickness and/or material of antiferromagnetic layer between the exchange biased free and exchange biased pinned layers, the initial angle of θ_f would be easily controlled by changing the direction of magnetic field during post-annealing in a magnetic field. We will demonstrate the experimental results of exchange biased free layer in the near feature.

4 Conclusions

We conducted a detailed study of H_{hard} dependence on CIMS in MgO-based MTJs with various junction sizes and various H_k. The decreases in J_c, J_{c0} and $E^{ave}/2k_BT$ are observed when applying H_{hard} for all MTJs except for the largest sample for which we measured CIMS. This result indicates that the reduction of J_c is attributable to both the increase of spin-transfer efficiency and the decrease in energy barrier in the case of applying H_{hard}. The estimated J_{c0} from the pulse duration dependence on J_c decreases with increase in the mutual angle between the direction of magnetization and the easy axis (θ_f), which is consistent with the theoretical prediction proposed by Slonczewski. The degree of the reduction of J_{c0} for the same value of H_{hard} decreases with decreasing size of MTJs. This behavior is considered to be related to not only the decrease in the mutual angle of magnetization due to the increase in anisotropy field H_k but also to the increase in the variance of the initial angle of magnetization θ_{FT} due to the thermally activated magnon excitation. The stable switching endurance related to CIMS was observed in a wide range of MTJ sizes when applying H_{hard}. This result indicates that by applying a magnetic field to a hard axis, the absolute value of the current that CIMS induces becomes smaller than the current value that the vortex state induces even in the largest sample with width of 350 nm. Moreover, we proposed a new architecture and a new switching method considering write disturbance. These results would be useful for application to spin memory and other spin-electronic devices.

References

1. J.C. Slonczewski, J. Magn. Magn. Mat. **159**, L1 (1996)
2. L. Berger, Phys. Rev. B **54**, 9353 (1996)
3. Y. Huai, F. Albert, P. Nguyen, M. Pakala, T. Valet, Appl. Phys. Lett. **84**, 3118 (2004)
4. Z. Li, S. Zhang, Phys. Rev. B **69**, 134416 (2004)
5. H. Kubota, A. Fukushima, Y. Ootani, S. Yuasa, K. Ando, H. Maehara, K. Tsunekawa, D.D. Djayaprawira, N. Watanabe, Y. Suzuki, Jpn J. Appl. Phys. **44**, L1237 (2005)
6. K. Yagami, A.A. Tulapurkar, A. Fukushima, Y. Suzuki, J. Appl. Phys. **97**, 10C707 (2005)
7. H. Kubota, A. Fukushima, Y. Ootani, S. Yuasa, K. Ando, H. Maehara, K. Tsunekawa, D.D. Djayaprawira, N. Watanabe, Y. Suzuki, IEEE Trans. Mag. **41**, 2633 (2005)
8. T. Inokuchi, H. Sugiyama, Y. Saito, K. Inomata, Appl. Phys. Lett. **89**, 102502 (2006); T. Inokuchi, H. Sugiyama, Y. Saito, K. Inomata, Intermag 2006 DC-06
9. T. Devolder, P. Crozat, J.-V. Kim, C. Chappert, K. Ito, J.A. Katine, M.J. Carey, Appl. Phys. Lett. **88**, 152502 (2006); C. Chappert, Intermag 2006 AA-04
10. J.Z. Sun, Phys. Rev. B **62**, 570 (2000)
11. J.C. Slonczewski, Phys. Rev. B **71**, 024411 (2005)
12. R.H. Koch, J.A. Katine, J.Z. Sun, Phys. Rev. Lett. **92**, 088302 (2004)
13. D. Lacour, J.A. Katine, N. Smith, M.J. Carey, J.R. Childress, Appl. Phys. Lett. **85**, 4681 (2004)
14. Z. Li, S. Zhang, Phys. Rev. B **69**, 134416 (2004)
15. Y. Saito, H. Sugiyama, K. Inomata, J. Appl. Phys. **97**, 10C914 (2005)
16. Y. Saito, H. Sugiyama, T. Inokuchi, K. Inomata, J. Magn. Magn. Mat. **303**, 34 (2006)
17. W. Park, I.J. Hwang, T. Kim, K.J. Lee, Y.K. Kim, J. Appl. Phys. **96**, 1748 (2004)
18. N. Stutzke, S.L. Burkett, S.E. Russek, Appl. Phys. Lett. **82**, 91 (2003)
19. Y. Liu, Z. Zhang, P.P. Freitas, J.L. Martins, Appl. Phys. Lett. **82**, 2871 (2003)
20. W.C. Jeong, J.H. Park, J.H. Oh, G.T. Jeong, H.S. Jeong, K. Kim, 2005 Symp. on VLSI Tech. Digest of Tech. Papers **10B-1**, 184 (2005)